

To appear in: P.A.S.P., February 1999

## LS Peg: A Low-Inclination SW Sextantis-Type Cataclysmic Binary with High-Velocity Balmer Emission Line Wings <sup>1</sup>

Cynthia J. Taylor, John R. Thorstensen,  
Department of Physics and Astronomy, Dartmouth College, 6127 Wilder Laboratories  
Hanover, NH 03755-3528; [cynthia.j.taylor](mailto:cynthia.j.taylor), [thorstensen@dartmouth.edu](mailto:thorstensen@dartmouth.edu)

and Joseph Patterson  
Department of Astronomy, Columbia University, 550 West 120th Street  
New York, NY 10027; [jop@astro.columbia.edu](mailto:jop@astro.columbia.edu)

### ABSTRACT

We present time-resolved spectroscopy and photometry of the bright cataclysmic variable LS Peg (= S193;  $V \approx 13.0$  – Szkody et al. 1997). The Balmer lines exhibit broad, asymmetric wings Doppler-shifted by about  $2000 \text{ km s}^{-1}$  at the edges, while the He I lines show phase-dependent absorption features strikingly similar to SW Sextantis stars, as well as emission through most of the phase. The C III/N III emission blend does not show any phase dependence. From velocities of  $H\alpha$  emission lines, we determine an orbital period of  $0.174774 \pm 0.000003 \text{ d}$  ( $= 4.1946 \text{ h}$ ), which agrees with Szkody's (1995) value of approximately 4.2 hours. No stable photometric signal was found at the orbital period. A non-coherent quasi-periodic photometric signal was seen at a period of  $20.7 \pm 0.3 \text{ min}$ .

The high-velocity Balmer wings most probably arise from a stream re-impact point close to the white dwarf. We present simulated spectra based on a kinematic model similar to the modified disk-overflow scenario of Hellier & Robinson (1994). The models reproduce the broad line wings, though some other details are unexplained.

Using an estimate of dynamical phase based on the model, we show that the phasing of the emission- and absorption-line variations is consistent with that in (eclipsing) SW Sex stars. We therefore identify LS Peg as a low-inclination SW Sex star.

Our model suggests  $i = 30^\circ$ , and the observed absence of any photometric signal at the orbital frequency establishes  $i < 60^\circ$ . This constraint puts a severe strain on interpretations of the SW Sex phenomenon which rely on disk structures lying slightly out of the orbital plane.

*Subject headings:* binary:close — stars:individual(LS Peg) — novae, cataclysmic variables

---

<sup>1</sup>Based in part on observations obtained at MDM Observatory, operated by Dartmouth College, Columbia University, the Ohio State University, and the University of Michigan.

## 1. Introduction

LS Peg (S193) was first identified as a cataclysmic variable (CV) by Downes & Keyes (1988). It is among the brightest CVs in the sky ( $V \approx 13.0$  – Szkody et al. 1997) which lacks a well-established orbital period. It is apparently a novalike system; such systems often show relatively high excitation emission lines, long-term brightness variations, and, in the case of the SW Sex stars, orbital variations in the narrow absorption components of He I and radial velocity phase shifts with respect to the photometric eclipse phase (Warner 1995; Thorstensen et al. 1991).

The classification of SW Sextantis (SW Sex) stars was created by Thorstensen et al. (1991). This classification has been somewhat controversial because it is based on spectroscopic properties while other variable-star classifications are based on photometric properties; therefore the SW Sex classification overlaps with other classifications (Dhillon 1996). SW Sex stars were originally defined as novalike variables with 1) eclipses, 2) orbital periods between 3 and 4 hours, 3) He II  $\lambda 4686$  emission around half the strength of  $H\beta$ , 4) a Balmer-line radial velocity phase that lags substantially behind the orbital phase, 5) absorption in Balmer and He I lines opposite the eclipse. This last characteristic is known as “phase 0.5 absorption”, referring to eclipse phase as phase  $\phi = 0$ . Over time, the definition has simplified somewhat, to: novalikes, with phase-dependent absorption around phase 0.5, in which the spectroscopic phase lags significantly behind the orbital phase (Warner 1995, Dhillon 1996). Since inclination depends on line of sight from Earth, the “eclipsing” characteristic has increasingly fallen away. In addition to the defining characteristics, SW Sex stars tend to have continuum and/or high-excitation lines eclipsed more strongly than low excitation lines (Warner 1995 and references therein; Young, Schneider, & Sheckman 1981; Baptista, Steiner, & Horne 1996), relatively narrow FWHM ( $\sim 1000 \text{ km s}^{-1}$ ) and large FWZI in the Balmer lines, no observable circular polarization (Young, Schneider, & Sheckman 1981; Grauer et al. 1994; Thorstensen et al. 1991; Dhillon & Rutten 1995; Stockman et al. 1992), and a radial temperature profile in the inner disk which is noticeably flatter than  $T \propto R^{-3/4}$  while in the high state (Baptista, Steiner, & Horne 1996; Rutten, van Paradijs, & Tinbergen 1992).

There is no single comprehensive study of LS Peg in the literature, but many observations have been published and we summarize these here. No stable photometric periods are known, but plenty of quasi-periodic oscillations have been seen in the light curve at different periods: a  $16.5 \pm 2$  min period from a one-night optical light curve, an intermittent 18.7 min period over several nights, a weaker quasi period at 32 min, and other possible periods ranging from 5 to 50 min (Garnavich, Szkody, & Goldader 1988; Garnavich & Szkody 1992; Szkody et al. 1994a). No significant circular polarization was detected (Stockman et al. 1992). Analysis of the Harvard plate collections from 1897 – 1988 showed long term high and low states of  $B \approx 12$  and  $B \approx 14$  (Garnavich & Szkody 1992). *IUE* and *Voyager* spectra of LS Peg in a high state were similar to SW Sex candidates V795 Her and PG0859+415 (BP Lyn), with all these showing deep UV absorption lines. The line ratios and slope of the UV flux distribution are not typical of dwarf novae at outburst. The low-state spectrum is most similar to 1H0551-819, with a flat flux distribution, only C IV and Mg II lines in emission, and Si III and N V in deep absorption (Szkody 1991; Szkody et al. 1997). No X-ray period

was determined from *Ginga* and *ROSAT* data, but the data place an upper limit of 40% on the sinusoidal amplitude. The differences in column densities and temperatures between the *ROSAT* and *Ginga* data indicated either a two-component system or a change of accretion characteristics (Szkody et al. 1994a; Szkody et al. 1994b). Szkody (1991) reported that the velocities of the Balmer-line wings  $< 50 \text{ km s}^{-1}$ , which implies a low inclination. In addition, very prominent, highly variable (on timescales  $< 10$  minutes), and random absorptions in He I  $\lambda 4471$  and Balmer emission were seen, with the absorption always redshifted by  $250\text{-}300 \text{ km s}^{-1}$ . By 1995, Balmer-line wings had appeared showing an extremely large velocity amplitude of  $\sim 1700 \text{ km s}^{-1}$ ; these were the only sinusoidal features seen (Szkody 1995). No orbital period has been formally published, but Szkody et al. (1994b) and Szkody (1995) refer to an orbital period of  $\sim 4.2$  hours from the Balmer emission-line wings.

## 2. Observations and Reductions

### 2.1. Spectroscopy

We used the telescopes at MDM Observatory on Kitt Peak, during five observing runs – 1996 July, 1996 September, 1996 October, 1996 December, and 1997 June. Table 1 lists the different combinations of telescopes, spectrographs, and CCD chips, as well as the spectral resolution (FWHM). The exposure times ranged from 5 to 8 minutes. The exact dates of observation are implicit in the radial velocity timeseries (Table 2). To avoid daily cycle count ambiguity, we observed over a wide range of hour angle. We derived the wavelength scale from comparison lamp spectra bracketing the observations as the telescope tracked. Flux standards were observed when conditions warranted.

For data reduction we used standard IRAF routines<sup>2</sup>. The pixel-to-wavelength transformations had typical RMS residuals of  $< 0.1 \text{ \AA}$ . The stability of the  $5577.350 \text{ \AA}$  night-sky line in the reduced data was  $< 5 \text{ km s}^{-1}$ , and the systematic uncertainty was on the order of  $10 \text{ km s}^{-1}$ . We estimate our flux calibrations to be accurate to about 30 per cent.

Because most of the lines have an asymmetric wing component, we could not use the standard algorithms described by Schneider & Young (1980) to measure the radial velocities. Since the base of the lines have an approximately constant width (see Figure 6) and the wings shift back and forth, the radial velocities were measured by hand using the midpoint of the full width zero intensity (FWZI). The spectra were first rectified using the IRAF task *sfit* and the FWZI were measured in *splot*. The times and velocities were corrected to the solar center.

Figure 1 shows results of a period search conducted using the ‘residual-gram’ method described by Thorstensen et al. (1996). The best fit is at 5.722 cycles/day. The Monte Carlo test of Thorstensen & Freed (1985) shows that the cycle count is unambiguous on all scales. A least-

---

<sup>2</sup>IRAF is distributed by the National Optical Astronomy Observatories.

squares sinusoid fit of

$$v(t) = \gamma + K \sin[2\pi(t - T_0)/P]$$

yielded

$$\begin{aligned} T_0 &= \text{HJD } 2450358.8964 \pm 0.0009, \\ P &= 0.174774 \pm 0.000003 \text{ d}, \\ K &= 593 \pm 21 \text{ km s}^{-1}, \\ \gamma &= -56 \pm 14 \text{ km s}^{-1}, \text{ and} \\ \sigma &= 183 \text{ km s}^{-1}, \end{aligned}$$

where  $\sigma$  is the uncertainty of a single measurement inferred from the goodness-of-fit.

Figure 2 shows the velocities derived from the H $\alpha$  wings folded on the best-fit period with the sinusoidal fit superposed. The  $K$  value is far too large for any plausible motion of the white dwarf. Interpreted literally, this  $K$  value yields a secondary mass function of  $f(M_2) = 3.77M_\odot$ , which, as an illustration, gives  $M_2 \gtrsim 30M_\odot$  assuming  $i = 30^\circ$  and  $M_1 = 0.7M_\odot$ .

## 2.2. Photometry

We carried out time-series photometry of LS Peg for 12 nights (distributed over an interval of 18 nights) in 1996 October, using the telescopes of the Center for Backyard Astrophysics (Harvey et al. 1995). We accumulated 55 hr of coverage, during which the star varied irregularly in the range  $V=12.5$ -13. A sample light curve is shown in the top frame of Figure 3.

We searched for periodic signals by calculating the power spectrum (from the discrete Fourier transform), and found no stable periods. The full amplitude upper limit to any signal in the vicinity of  $P_{\text{orb}}$  was 0.04 mag, and the upper limit at  $P_{\text{orb}}$  exactly was 0.027 mag.

The individual nights showed features in the power spectrum near 70 cycles  $\text{d}^{-1}$ , and a weighted average over the 6 longest nights of coverage yielded the mean power spectrum in the lower frame of Figure 3. The highest peak occurs at a period of  $20.7 \pm 0.3$  min, and corresponds to a full amplitude of 0.041 mag in the 12-night time series. However, the structure and precise location of the peak are not stable, but drift about on a timescale of hours. Thus this is probably a manifestation of the signal reported at 19 min by Garnavich & Szkody (1992), with the period difference merely arising from erratic drifts in the star. Since the signal is not stable in phase, the measured amplitude of 0.041 mag underestimates the true amplitude of the (incoherent) signal, which occasionally appears to reach 0.2 mag in the raw light curve.

In CV parlance, such things are called quasi-periodic oscillations (QPOs). They are commonly seen in novalike variables (TT Ari: Andronov et al. 1998; V795 Her: Zhang et al. 1991; AH Men: Patterson 1995), and are oddly clustered near 20 min. But there is still no understanding of the origin of these signals.

### 3. Analysis of Spectra

Figure 4 is an average of 23 spectra from the 1996 October run. The spectrum has typical CV lines (see Table 3), including the C III and N III blend near  $\lambda 4640$ . There are two weak unidentified lines at approximately  $\lambda 5000$  and  $\lambda 6344$ . The line near  $\lambda 5000$  is most likely a N II blend. The feature near  $\lambda 6344$  could be due to Si I or Mg I. Interstellar Na D lines are also present.

We spend most of this section discussing phase-dependent features in the line profiles which reproduce from orbit to orbit, but the profiles also show secular variations. Figure 5 shows rectified spectra from four different orbits at phase  $\phi = 0.7$ . The middle two spectra show absorption in the H $\alpha$  and H $\beta$  line wings as well as in the He I  $\lambda 6678$  and  $\lambda 4920$  lines, but the upper and lower spectra show little or no absorption. In our data, the most pronounced orbit-to-orbit variation occurs roughly between phases  $\phi_{\text{spec}} \sim 0.65 - 0.85$ , with slight variations mainly in the He I lines at other phases. These line profile variations are evidently due to the variable phasing of the appearance and disappearance of the absorption features. Szkody & Piché (1990) have seen these variations in the SW Sex stars DW UMa, SW Sex, and V1315 Aql.

Figures 6-8 show single-trailed spectra of LS Peg. The single-trailed image was constructed by taking 155 continuum-subtracted spectra from the 1996 September and October runs, computing phases from the ephemeris above, and binning the spectra into 150 phase bins, each of which corresponds to a horizontal line in the image. To compute the spectrum in each phase bin, spectra falling near the central phase of the bin were combined using weights computed from a Gaussian in phase, with  $\sigma = 0.02$  cycle. Thus a feature appearing in one input spectrum will be smeared over several lines of the image. The image lines were stacked to create the 2-D trailed spectrum with the first 50 lines repeated to provide continuity. Note that since there is no eclipse by the secondary, the phase is based on the blue-to-red crossing of the broad wings, as described above.

In Figure 6 the broad emission wings in the Balmer lines are quite prominent. The width of the emission wings remains approximately constant. The He I lines all show braided emission and absorption features, with the absorption crossing over at phase 0.65–0.9, suggestive of SW Sex stars. The Fe II  $\lambda 5169$  line shows a similar braided feature. There also seems to be a faint, broad, high-velocity ( $\sim 1500 \text{ km s}^{-1}$ ), blueshifted emission feature in the He I lines starting at phase 0.4 and ending around phase 1.05; it is most prominent in  $\lambda 5876$  (see Figure 7), and is barely visible in  $\lambda 6678$ ,  $\lambda 5015$ , and  $\lambda 4920$ . Unfortunately, the interstellar Na D lines obscure any possible corresponding redshifted emission of  $\lambda 5876$ , though close examination of the other lines suggests that there is no redshifted emission. Also, the He I absorption crosses from red to blue at phase  $\approx 0.8$ . Both the C III/N III blend and He II lines show no phase-dependent features. The constant velocity and sharpness of the Na D lines confirms that they are interstellar.

Figure 8 is a close-up of the H $\alpha$  and He I  $\lambda 6678$  region of the single trailed spectrum. The H $\alpha$  wings extend out to  $\pm 2000 \text{ km s}^{-1}$  and have a width of approximately  $3000 \text{ km s}^{-1}$ . At phases  $\phi \approx 0.75 - 0.85$ , there is relatively strong blueshifted absorption in the H $\alpha$  wing and the edge of the line core. This occurs at the same phase as the He I absorption red-to-blue crossing, most strongly

seen in Figure 7. There appears to be fainter redshifted absorption in the  $H\alpha$  wing and line core at phase  $\phi \approx 0.25$ . The faint, broad, high-velocity, blueshifted emission in  $\lambda 6678$  occurs at the same phase as the blueshifted  $H\alpha$  wing. Note that the maximum blueshift of the faint emission in  $\lambda 6678$  occurs at the same phase as absorption crossing from red to blue (see Figure 7 for a clearer example in  $\lambda 5876$ ).

#### 4. Doppler Tomography

We created Doppler tomograms of  $H\alpha$  (Figure 9) and He I  $\lambda 6678$  (Figure 10) using the Fourier-filtered back-projection algorithm (Marsh & Horne 1988, Horne 1991). Unlike the Maximum Entropy Method (MEM) algorithm, the Fourier-filtered back-projection algorithm does not require only positive values in the single-trailed spectrum (see the appendix of Harlaftis & Marsh 1996 for a comparison of the two algorithms).

We subtracted unity from our single-trailed spectrum (which was created from continuum-divided spectra) to obtain a mean of zero, as required by the Doppler tomogram algorithm. The Doppler tomogram is not very sensitive to the assumed system parameters; we took  $M_1 = 0.7M_\odot$ ,  $M_2 = 0.39M_\odot$ ,  $K_1 = 120 \text{ km s}^{-1}$ ,  $K_2 = 215 \text{ km s}^{-1}$ , and  $i = 30^\circ$ .  $M_1$  and  $K_1$  are plausible values for SW Sex stars,  $M_2$  is determined from the mass-period relationship ( $M_2 = 0.065P_{\text{orb}}^{5/4}(\text{h})$ ; Warner 1995), and  $i$  is determined from our model described in §5. The model was also used to estimate the orbital phasing, so the tomograms could be rotated slightly.

The difference between the  $H\alpha$  core and wing tomograms is shown in Figure 9. The core tomogram (lefthand panel) is similar to V795 Her (Casares et al. 1996; Dickinson et al. 1997), PX And (Hellier & Robinson 1994; Still, Dhillon, & Jones 1995), and V1315 Aql (Dhillon, Marsh, & Jones 1991; Hellier 1996). It suggests that the line core emission is from the disk edge. The wing tomogram (righthand panel) is most similar to V795 Her wing tomogram (Figure 13b in Dickinson et al. 1997), and to a lesser extent, SW Sex (Dhillon, Marsh, & Jones 1997) and V1315 Aql (Hellier 1996). The high-velocity wing emission appears to originate from both the stream and the inner disk suggesting the stream-disk interaction at the re-impact site in the disk-overflow models. However, the exact stream trajectory is uncertain since we don't know  $K_1$ . The circular pattern is an artifact of the phase-smearing noise in the single-trailed spectra. The predicted single-trailed spectra reasonably match the data, which suggests the emission is near the plane of the disk.

In our He I  $\lambda 6678$  tomogram (Figure 10), and to a lesser extent in the  $H\alpha$  tomograms, we violate the basic premise of Doppler tomography: that the emission/absorption is seen at all phases. This violation is clearly seen in Figure 10 in the predicted trailed spectrum, in which the absorption extends in phase to produce more of an “S” wave not seen in the original data. The emission is similar to V795 Her  $\lambda 6678$  tomograms (Casares et al. 1996; Haswell et al. 1994). The absolute phasing is not known in LS Peg or V795 Her, so again some rotation of the tomograms may occur.

## 5. Model

In an effort to understand the origin of the very high-velocity Balmer-line wings, we used a modified version of the disk-overflow model of Hellier and Robinson (1994). Our purpose was not to exhaustively explore parameter space, nor to consider radiative transfer problems, but simply to arrive at a plausible kinematic model. The stream motions were approximated by particle trajectories, which were computed in a Roche potential using code described by Thorstensen et al. (1991). The stellar masses were held fixed at plausible values ( $M_1 = 0.7M_\odot$ ,  $M_2 = 0.39M_\odot$ ). In Hellier & Robinson’s scenario, a portion of the accretion stream flows over the top of the disk and strikes the disk close to the white dwarf. At the point where the stream re-impacts the disk, we assumed the emission to be a broad Gaussian with a  $\sigma$  equal to 50% of the average of the Keplerian disk and the stream free-fall velocities. As in Hellier and Robinson’s model, our re-impact region is slightly upstream from the re-impact point interpolated from Table 1 in Lubow (1989) for our adopted parameters. We also assume that prior to re-impact the stream creates absorption, which we model as a narrower Gaussian with  $\sigma$  equal to 25% of the free-fall velocity. We then added a double-peaked Keplerian disk profile. Note that in the model, zero phase corresponds to inferior conjunction of the secondary, while the phase of the fit to the broad line wing motion in the data (hereafter the “data phase”) has no clear dynamical interpretation. Our simulations bore a reasonable resemblance to the data using  $i = 30^\circ$ , disk radius =  $3.5 \times 10^{10}$  cm, and stream re-impact region  $6.33 - 6.05 \times 10^9$  cm from the white dwarf.

Figures 11 and 12 show comparisons of the single-trailed  $H\alpha$  spectrograms and model. The model phase was matched by eye to the data phase. The model matches the gross features we observe, in particular the very high velocity broad wings of the Balmer lines. It does not explain, however, the relatively strong absorption in the wing and edge of the line core at data phase  $\approx 0.8$  (model phase  $\approx 1.4$ ) and to a lesser extent at data phase  $\approx 0.25$  (model phase  $\approx 0.85$ ). Also, in the model the line core shows an orbital sinusoidal velocity variation, while the observed line core remains at nearly constant velocity (see Figure 12). The absorption in phase with the emission wings suggests some absorption associated with the re-impact point. However when we extended the absorption along the entire stream to include the re-impact region as in the model of V795 Her by Dickinson et al. (1997), we get absorption in the broad wings at later phases than that is seen in the data. But it is important to note that our model is relatively simple.

How does this system compare to others in which large-amplitude motion and absorption effects occur? The effects seen in the SW Sex stars are referred in phase to the eclipse (SW Sex stars as defined by Thorstensen et al. (1991) always show eclipses). Because LS Peg does not eclipse, we do not know the absolute orbital phase. However, our model is computed using mass points to generate the potential, so the orbital phase in the model is always known to arbitrary accuracy. Our model is matched by eye to the data, giving a rough relationship between orbital phase and spectroscopic phase. To the extent our model is realistic, we can ask whether the line wing motion might be offset in phase from the ‘expected’ motion of the white dwarf center of mass, and whether the He I absorption events occur opposite the expected ‘eclipse’ phase. Both these

effects are seen in SW Sex stars (Thorstensen et al. 1991).

Using the by-eye match between the model and our spectroscopic ‘data phase’ (for which  $\phi = 0$  at blue-to-red crossing), the inferior conjunction of the red star (which would yield an eclipse in a high-inclination system) occurs at data phase 0.4. If the line base traced the white dwarf motion (unlikely in this case, but often assumed), the eclipse would be expected at data phase 0.5. Thus the spectroscopic phase ‘lags’ the phase expected for white-dwarf motion by  $\sim 0.1$  cycle. The sense of the offset is the same as seen in SW Sex stars, but it is somewhat smaller than the offsets seen in most SW Sex stars, in which offsets of 0.15 to 0.2 cycles are common (Garnavich et al. 1990; Honeycutt et al. 1986; Thorstensen et al. 1991; Casares et al. 1996). Again using the model-to-data phase offset, we find that He I absorption occurring opposite the eclipse would appear around data phase  $\phi = 0.9$ . The absorption is actually seen near data phase  $\phi = 0.8$ . In view of the uncertain correspondence between binary phase and data phase, this is fair agreement; alternatively, the match to standard SW Sex behavior could be improved for both the line motion and the absorption if a slightly different phase offset were assumed.

The model suggests, then, that the relationship between dynamical (eclipse) phase and spectroscopic phase is similar to that found in SW Sex stars. The absorption seen in the He I lines also superficially resembles that seen in SW Sex stars. To explore how accurately the absorption in LS Peg resembles the SW Sex phenomenon, we constructed Figure 13, which compares the LS Peg spectrogram to a single-trailed spectrogram of PX And, which was constructed from data obtained 1988 December and 1989 February (already discussed by Thorstensen et al. 1991). The PX And data are of lower spectral resolution than the present LS Peg data, but the presentation is otherwise similar. The resemblance between behaviors of the He I  $\lambda 5015$  absorption in these two stars is detailed and striking. Note especially in PX And how the weak redshifted absorption appears soon after eclipse, grows in strength, and moves toward the blue, with maximum strength occurring opposite the eclipse. The absorption in LS Peg mimics this behavior perfectly.

Note that  $\phi_{\text{spec}}$  is plotted on the left axes of both panels; these phases are derived from fits to the  $H\alpha$  velocities, and the two panels are aligned with respect to this phase. The eclipse phase plotted for PX And is derived from the observed eclipse, whereas (again) the LS Peg eclipse phase is *inferred* from the dynamical model of the emission lines. Again, there is fair agreement between these two left axes – they differ by 0.11 cycle. Table 4 gives the estimated phases of the He I absorption events in both stars in both phase conventions.

In an attempt to constrain the absorption phases, Hellier (1998) adds a flared disk to the disk-overflow model and, unlike the previous versions of the model, includes spatial obscuration of the disk and stream by the secondary, obscuration of parts of the disk by the stream, obscuration of the stream by a flared disk, and obscuration of the stream by other other regions of the stream. Previous versions of the model (Hellier & Robinson 1994; Hellier 1996) produced the absorption features at all phases. In Hellier’s recent model, the strength and phase dependence of the absorption depends on the departure of  $i + \alpha$  from  $90^\circ$ , where  $i$  is the inclination and  $\alpha$  is the flare angle of the disk.



He found if  $i + \alpha \lesssim 80^\circ$ , the phase-dependent absorption features weaken and become visible at all phases. Based on theoretical and observational estimates, Hellier assumes a flare angle,  $\alpha \approx 4^\circ$ .

We can estimate an upper limit for the inclination of LS Peg. The firmest limit comes from the absence of eclipses. Because we don't know the exact masses, we use the values assumed in our model,  $M_1 = 0.7M_\odot$  and  $M_2 = 0.39M_\odot$ , and estimate from Table 1 in Bailey (1990) that  $i \approx 72^\circ$ , which corresponds to a grazing eclipse. For Hellier's model to work at this inclination, the flare angle must be greater than  $8^\circ$ , at least twice as large as the theoretical and observational estimates. In fact, the inclination of LS Peg is probably much lower than  $72^\circ$  since there is no photometric signal at the orbital period. Our model provides a reasonable fit at an inclination of  $30^\circ$ , which would imply an unrealistic flare angle of over  $50^\circ$ .

## 6. Conclusion and Discussion

We obtain a radial velocity period of  $0.174774 \pm 0.000003$  d. This is almost certainly the orbital period.

The phase-dependent absorption is reminiscent of SW Sex stars, and a comparison between our data, our model, and archival data of the well-studied SW Sex star PX And suggests that the absolute binary phase in LS Peg is about as expected for the SW Sex phenomenon. There is a striking qualitative resemblance between the phase-dependent He I absorption features observed in LS Peg and those observed in SW Sex stars.

As new objects are discovered, the SW Sex behaviors listed by Thorstensen et al. (1991) continue to appear together as a suite. Although eclipses are formally necessary in the original definition of SW Sex stars, phase-dependent He I absorption appears to be fairly common in non-eclipsing bright novalikes (such as WX Ari; Beuermann et al. 1992). The formal criterion that a system be eclipsing for admission to the SW Sex class was always somewhat unsatisfactory, as it depends on our accidental viewing angle rather than on a physical characteristic of the system; in this sense the phase-dependent absorption features are a more fundamental criterion. We believe that LS Peg should be classified as an SW Sex star even though it does not eclipse.

The (modest) success of our simple kinematic model in accounting for the broad line wings – and the indirect evidence that the absolute binary phase predicted by the model is as expected given the behavior of other SW Sex stars – suggests strongly that the disk-overflow model proposed by Hellier & Robinson (1994) is essentially correct. The striking broad line wings seen in Figures 6, 8, and 11 are almost certainly coming from material associated with the stream overflowing the disk and the stream re-impact point.

However, as Casares et al. (1996) pointed out, Hellier & Robinson's disk-overflowing stream scenario does not limit the phase of the absorption to around  $\phi \sim 0.5$ . The inclination of LS Peg is so low that a flared disk such as that proposed by Hellier (1998) *cannot* explain the phase

dependence of the absorption, so a new explanation must be sought. A clue may come from recent hydrodynamical simulations of the stream-disk interaction by Armitage & Livio (1996, 1998). For inefficient cooling, an explosive stream-disk interaction produces a “halo” of material above and below the disk as well as a bulge along the disk rim downstream of the stream impact. Because of the surface brightness of the disk is highest toward its center, the absorption produced by such out-of-plane material could be highly dependent on viewing angle.

We see no evidence of a strictly periodic modulation in the photometry. In view of the lack of polarization, the lack of a strict photometric period, and the similarity to SW Sex stars (none of which are known to be magnetic), there is little to corroborate suggestions that this is a magnetic CV. Thus we can consider it unlikely that the magnetic accretion models of Casares et al. (1996) and Williams (1989) apply in this case.

We warmly thank Bob Fried at Braeside Observatory and the Columbia University Astronomy C3997 Fall 1995 class for taking the photometric data. We also thank Keith Horne for providing the Fourier-filtered back-projection Doppler tomography code. We thank the NSF for support through grant AST-9314787 and the MDM staff for their usual excellent support. This research made use of the Simbad database, operated at CDS, Strasbourg, France.

## REFERENCES

- Andronov, I.L. et al. 1998, AJ, in press
- Armitage, P.J. & Livio, M. 1996, ApJ, 470, 1024
- Armitage, P.J. & Livio, M. 1998, ApJ, 493, 898
- Bailey, J. 1990, MNRAS, 243, 57
- Baptista, R., Steiner, J.E., & Horne, K. 1996, MNRAS, 282, 99
- Beuermann, K., Thorstensen, J.R., Schwöpe, A.D., Ringwald, F.A., & Sahin, H. 1992, A&A, 256, 442
- Casares, J., Martinez-Pais, I.G., Marsh, T.R., Charles, P.A., & Lazaro, C. 1996, MNRAS, 278, 219
- Dhillon, V. 1996, in Cataclysmic Variables and Related Objects, ed. Evans, A. & Wood, J. H. (Dordrecht: Kluwer Academic), 3
- Dhillon, V.S., Marsh, T.R., & Jones, D.H.P. 1991, MNRAS, 252,342
- Dhillon, V.S., Marsh, T.R., & Jones, D.H.P. 1997, MNRAS, 291,694
- Dhillon, V.S. & Rutten, R.G.M. 1995, MNRAS, 277, 777
- Dickinson, R.J., Prinja, R.K., Rosen, S.R., King, A.R., Hellier, C., & Horne, K. 1997, MNRAS, 286, 447
- Downes, R.A. & Keyes, C.D. 1988, AJ, 96, 777
- Garnavich, P., Szkody, P., & Goldader, J. 1988, BAAS, 20, 1020
- Garnavich, P.M., Szkody, P., Mateo, M., Feinswog, L., Booth, J., Goodrich, B., Miller, H.R., Carini, M.T., & Wilson, J.W. 1990, ApJ, 365, 696
- Garnavich, P., & Szkody, P. 1992, AAVSO J, 21, 81
- Grauer, A.D., Ringwald, F.A., Wegner, G., Liebert, J., Schmidt, G.D., & Green, R.F. 1994, AJ, 108, 214
- Harlaftis, E.T. & Marsh, T.R. 1996, A&A, 308, 97
- Harvey, D., Skillman, D., Patterson, J., & Ringwald, F.A. 1995, PASP, 107, 551
- Haswell, C., Horne, K., Thomas, G., Patterson, J., & Thorstensen, J.R. 1994, in Interacting Binary Stars, ASP Conference Series Vol. 56, ed. A Shafter (San Francisco, Astronomical Society of the Pacific), p. 268
- Hellier, C. 1996, ApJ, 471, 949
- Hellier, C. & Robinson, E.L. 1994, ApJ, 431, L107
- Honeycutt, R.K., Schlegel, E.M., & Kaitchuck, R.H. 1986, ApJ, 302, 388
- Horne, K. 1991 in Fundamental Properties of Cataclysmic Variable Stars: Proc. 12th North American Workshop on Cataclysmic Variables and Low Mass X-Ray Binaries, ed. A. W. Shafter (San Diego, San Diego State Univ.), p. 23

- Lubow, S.H. 1989, ApJ, 340, 1064
- Marsh, T.R. & Horne, K. 1988, MNRAS, 235, 269
- Patterson, J. 1995, PASP, 107, 657
- Rutten, R.G.M., van Paradijs, J., & Tinbergen, J. 1992, A&A, 260,213
- Still, M.D., Dhillon, V.K., Jones, D.H.P. 1995, MNRAS, 273, 863
- Stockman, H.S., Schmidt, G.D., Berriman, G., Liebert, J., Moore, R.L., & Wickramasinge, D.T. 1992, ApJ, 401, 628
- Szkody, P. 1991, in Fundamental Properties of Cataclysmic Variable Stars, ed. A. Shafter (San Diego, San Diego State University), p. 56
- Szkody, P. 1995, in Cape Workshop on Magnetic Cataclysmic Variables, ASP Conference Series Vol. 85, ed. D. A. H. Buckley & B. Warner (San Francisco, Astronomical Society of the Pacific), p. 54
- Szkody, P., Hoard, D.W., Patterson, J., Moulden, M., Howell, S., & Garnavich, P. 1994a, in Interacting Binary Stars, ASP Conference Series Vol. 56, ed. A Shafter (San Francisco, Astronomical Society of the Pacific), p. 350
- Szkody, P., Garnavich, P., Castelaz, M., & Makino, F. 1994b, PASP, 106, 616
- Szkody, P., Garnavich, P., Holberg, J., Silber, A., & Pastwick, L. 1997, AJ, 113, 2276
- Szkody, P. & Piché, F. 1990, ApJ, 361, 235
- Schneider, D. & Young, P. 1980, ApJ, 238, 946
- Thorstensen, J.R. & Freed, I.B. 1985, AJ, 90, 2082
- Thorstensen, J.R., Ringwald, F.A., Wade, R.A., Schmidt, G.D., & Norsworthy, J.E. 1991, AJ, 102, 272
- Thorstensen, J.R., Patterson, J.O., Shambrook, A., & Thomas, G. 1996, PASP, 108, 73
- Warner, B. 1995, Cataclysmic Variable Stars (Cambridge, Cambridge University Press)
- Williams, R.E. 1989, AJ, 97, 1752
- Young, P., Schneider, D.P., & Shetman, S.A. 1981, ApJ, 244,259
- Zhang, E., Robinson, E.L., Ramseyer, T.F., Shetrone, M.D., & Stiening, R.F. 1991, ApJ, 381, 534

Table 1. Observation Log

| Dates (UT) | No. of Spectra | Telescope (m) | Spectr. | CCD                               | $\lambda$ range ( $\text{\AA}$ ) | FWHM ( $\text{\AA}$ ) |
|------------|----------------|---------------|---------|-----------------------------------|----------------------------------|-----------------------|
| 1996 Jul.  | 19             | 2.4           | modular | Tek 1024 <sup>2</sup> thinned     | 4610 - 6688                      | 3                     |
| 1996 Sep.  | 71             | 1.3           | MkIII   | Loral 2048 <sup>2</sup> unthinned | 4310 - 7184                      | 5                     |
| 1996 Oct.  | 68             | 2.4           | modular | Loral 2048 <sup>2</sup> unthinned | 4585 - 7171                      | 3                     |
| 1996 Dec.  | 17             | 1.3           | MkIII   | Tek 1024 <sup>2</sup> thinned     | 4472 - 6760                      | 5                     |
| 1997 Jun.  | 4              | 2.4           | modular | Tek 2048 <sup>2</sup> thinned     | 4000 - 7502                      | 3.5                   |

Table 2. LS Peg H $\alpha$  Line Based Radial Velocities

| HJD <sup>a</sup> | V<br>(km s <sup>-1</sup> ) | HJD <sup>a</sup> | V<br>(km s <sup>-1</sup> ) | HJD <sup>a</sup> | V<br>(km s <sup>-1</sup> ) | HJD <sup>a</sup> | V<br>(km s <sup>-1</sup> ) |
|------------------|----------------------------|------------------|----------------------------|------------------|----------------------------|------------------|----------------------------|
| 266.9369         | -770                       | 347.6384         | -354                       | 353.8180         | -486                       | 358.8963         | 3                          |
| 266.9413         | -738                       | 347.6441         | -761                       | 353.8220         | -385                       | 359.7101         | -477                       |
| 266.9463         | -565                       | 347.6525         | -555                       | 353.8260         | -152                       | 359.7127         | -796                       |
| 267.9184         | 125                        | 347.6582         | -615                       | 353.8300         | -79                        | 359.7153         | -609                       |
| 267.9248         | -21                        | 347.6639         | -879                       | 353.8339         | 473                        | 359.7643         | -331                       |
| 267.9292         | -117                       | 347.6696         | -637                       | 353.8379         | 583                        | 359.7690         | -308                       |
| 267.9404         | -409                       | 347.7694         | 642                        | 353.8419         | 400                        | 359.7737         | -125                       |
| 267.9458         | -670                       | 347.7751         | 404                        | 354.8731         | -221                       | 359.7783         | 240                        |
| 269.9007         | -592                       | 347.7808         | 336                        | 354.8771         | -253                       | 359.8520         | 222                        |
| 269.9044         | -505                       | 347.7865         | -25                        | 354.8810         | -20                        | 359.8546         | 154                        |
| 269.9073         | -459                       | 347.7922         | 43                         | 355.8596         | -331                       | 359.8572         | 195                        |
| 270.8751         | 404                        | 347.7979         | -112                       | 355.8635         | -116                       | 359.8597         | -239                       |
| 270.8794         | 248                        | 347.8061         | -345                       | 355.8675         | -454                       | 359.8623         | -152                       |
| 270.8999         | -208                       | 347.8118         | -674                       | 356.8681         | 496                        | 359.8649         | -239                       |
| 270.9042         | -281                       | 347.8175         | -715                       | 356.8721         | 144                        | 359.8675         | -426                       |
| 270.9122         | -427                       | 347.8232         | -432                       | 356.8761         | 341                        | 359.8701         | -262                       |
| 270.9179         | -651                       | 347.8289         | -491                       | 356.8800         | 163                        | 359.8727         | -394                       |
| 270.9772         | -446                       | 347.8347         | -665                       | 356.8840         | 108                        | 359.8753         | -504                       |
| 270.9816         | -263                       | 347.8423         | -615                       | 356.8880         | -57                        | 360.5978         | -650                       |
| 346.7405         | 413                        | 347.8480         | -710                       | 356.8919         | -253                       | 360.6018         | -806                       |
| 346.7462         | 199                        | 347.8537         | -519                       | 356.8959         | -349                       | 360.6057         | -737                       |
| 346.7519         | -158                       | 347.8595         | -432                       | 356.8999         | -280                       | 360.6097         | -486                       |
| 346.7576         | 121                        | 347.8652         | -569                       | 356.9038         | -513                       | 360.6137         | -550                       |
| 346.7633         | -190                       | 347.8709         | -372                       | 357.7301         | 629                        | 434.5914         | 577                        |
| 346.7691         | -372                       | 350.8049         | -829                       | 357.7353         | 446                        | 434.5968         | 70                         |
| 346.7785         | -578                       | 350.8106         | -587                       | 357.7379         | 496                        | 434.6022         | 476                        |
| 346.7842         | -482                       | 350.8171         | -633                       | 357.7405         | 350                        | 435.5937         | -588                       |
| 346.7899         | -692                       | 350.8228         | -363                       | 357.7430         | 368                        | 435.5991         | -341                       |
| 346.7956         | -432                       | 350.8343         | -414                       | 357.8829         | 126                        | 435.6046         | -643                       |
| 346.8013         | -414                       | 350.8475         | -144                       | 357.8855         | -253                       | 435.6100         | -414                       |
| 346.8070         | -528                       | 350.8532         | -7                         | 357.8907         | -79                        | 438.5739         | -560                       |
| 346.8156         | -578                       | 350.8589         | -25                        | 357.8932         | 368                        | 438.5793         | -506                       |
| 346.8270         | -121                       | 350.8646         | 121                        | 357.8958         | 186                        | 438.5847         | -241                       |
| 346.8327         | -94                        | 351.7244         | -235                       | 358.8452         | -417                       | 438.5901         | -99                        |
| 346.8384         | 34                         | 351.7301         | -149                       | 358.8484         | -641                       | 440.5717         | 499                        |
| 346.8441         | -130                       | 351.7358         | 94                         | 358.8517         | -678                       | 440.5771         | 335                        |
| 346.8521         | -16                        | 351.7415         | 491                        | 358.8550         | -618                       | 440.5825         | 454                        |
| 346.8578         | 34                         | 351.7472         | 683                        | 358.8648         | -532                       | 440.5879         | 47                         |
| 346.8635         | 683                        | 351.7529         | 217                        | 358.8681         | -532                       | 440.5933         | -158                       |
| 346.8692         | 642                        | 351.7607         | 683                        | 358.8747         | -230                       | 440.5987         | 326                        |
| 346.8749         | 701                        | 351.7664         | 578                        | 358.8797         | -417                       | 626.9807         | -710                       |

Table 2—Continued

| HJD <sup>a</sup> | V<br>(km s <sup>-1</sup> ) | HJD <sup>a</sup> | V<br>(km s <sup>-1</sup> ) | HJD <sup>a</sup> | V<br>(km s <sup>-1</sup> ) | HJD <sup>a</sup> | V<br>(km s <sup>-1</sup> ) |
|------------------|----------------------------|------------------|----------------------------|------------------|----------------------------|------------------|----------------------------|
| 347.6156         | 258                        | 351.7721         | 623                        | 358.8832         | -79                        | 627.9839         | -371                       |
| 347.6213         | 157                        | 351.7778         | 760                        | 358.8865         | -2                         | 628.9923         | 145                        |
| 347.6270         | -149                       | 351.7835         | 569                        | 358.8898         | 76                         | 629.9859         | 515                        |
| 347.6327         | -459                       | 351.7892         | 569                        | 358.8930         | -2                         |                  |                            |

<sup>a</sup>Heliocentric JD of mid-integration minus 2450000.

Table 3. Equivalent Widths

| Lines                             | EW ( $\text{\AA}$ ) |
|-----------------------------------|---------------------|
| H $\alpha$                        | 12.6                |
| H $\beta$                         | 2.6                 |
| He I $\lambda 6678$               | 0.2                 |
| He I $\lambda 5015$               | 0.2                 |
| He I $\lambda 4920$               | 0.1                 |
| He II $\lambda 4686$              | 0.6                 |
| C III+N III $\lambda 4640 - 4650$ | 0.5                 |
| Fe II $\lambda 5169$              | 0.2                 |
| Fe II $\lambda 5317$              | 0.1                 |
| $\lambda 5000^a$                  | 0.2                 |
| $\lambda 6344^b$                  | 0.1                 |

<sup>a</sup>Possible blend of N II.

<sup>b</sup>Si I? or Mg I?

Table 4. LS Peg and PX And He I  $\lambda 5015$  Phase Measurements

|                       | PX And              |                      | Model               | LS Peg               |
|-----------------------|---------------------|----------------------|---------------------|----------------------|
|                       | $\phi_{\text{ecl}}$ | $\phi_{\text{spec}}$ | $\phi_{\text{ecl}}$ | $\phi_{\text{spec}}$ |
| inferior conj.        | 0.0                 | 0.29                 | 0.0                 | 0.40                 |
| start of deeper absn  | 0.41                | 0.70                 | $[0.23]^a$          | 0.63                 |
| center of deeper absn | 0.44                | 0.79                 | $[0.31]^a$          | 0.71                 |

<sup>a</sup>Estimated from Figure 10.



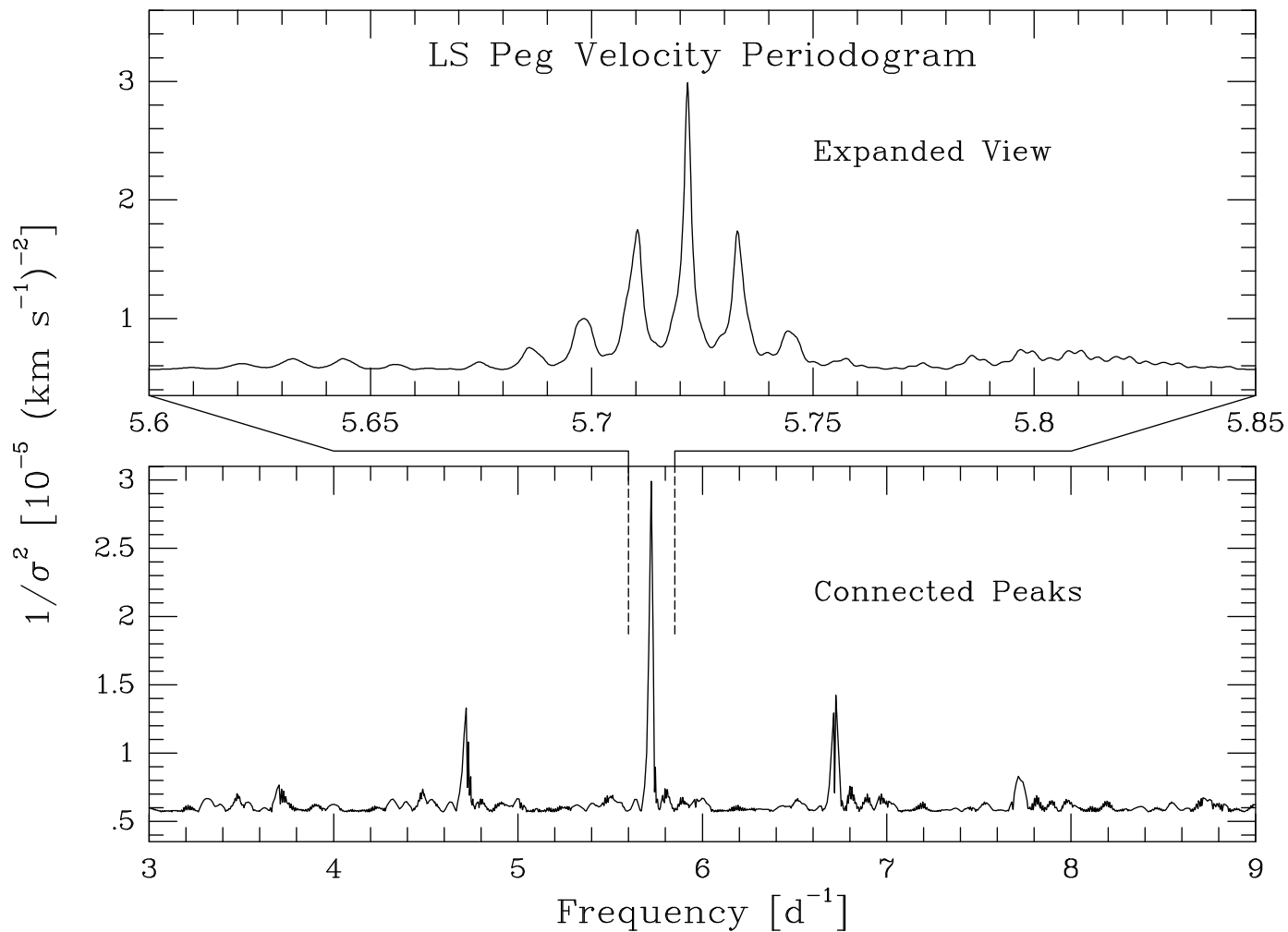


Fig. 1.— Periodogram of velocities of LS Peg. The lower panel shows the upper envelope of the periodogram, created by joining local maxima with straight lines, while the upper shows a magnified view of the region of the highest peak.

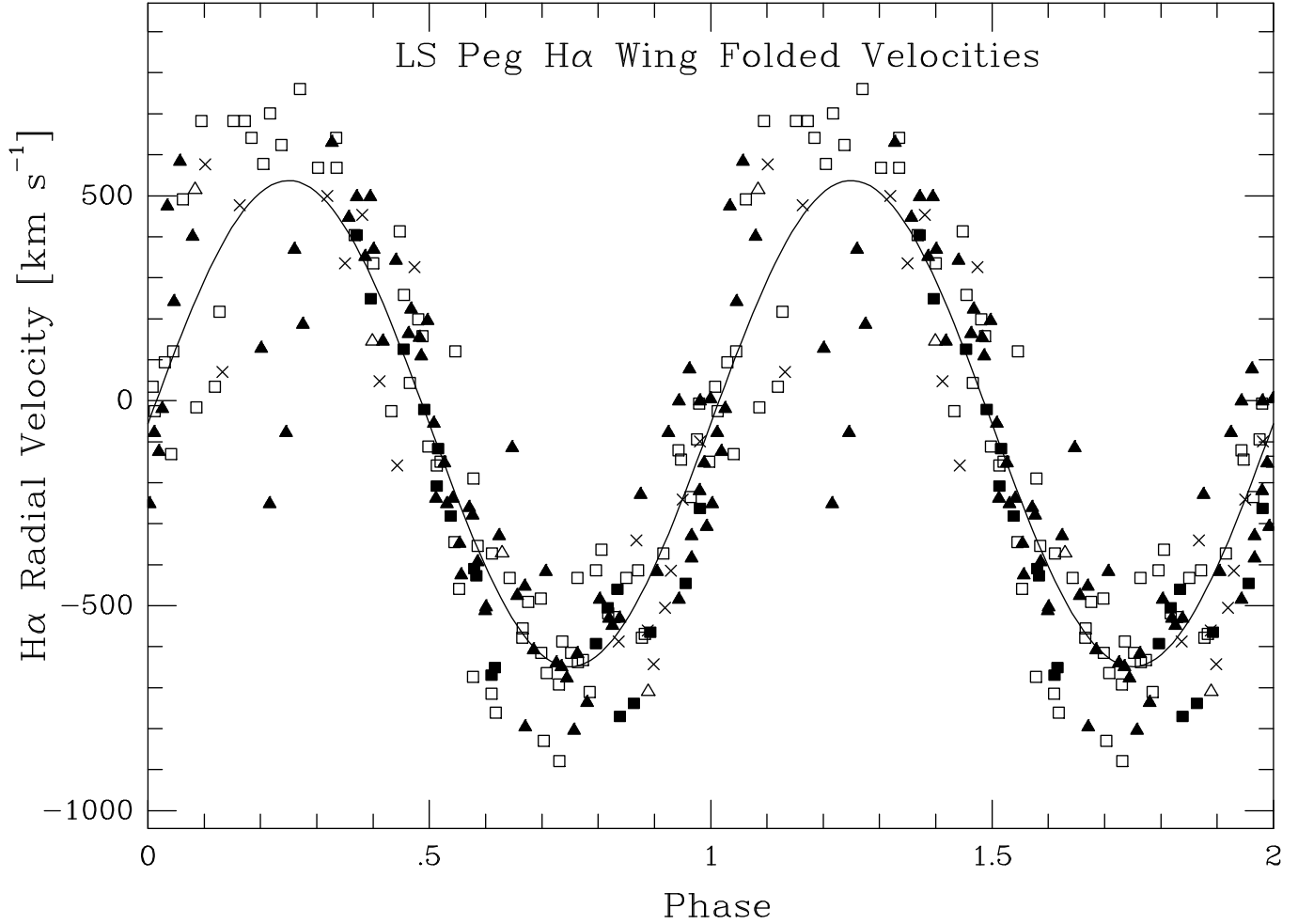


Fig. 2.— H $\alpha$  radial velocities derived from the broad emission wings folded on the ephemerides given in text. Two cycles are plotted for continuity, and the best-fit sinusoid is shown. The symbols are: solid squares, 1996 July; squares, 1996 September; solid triangles, 1996 October; crosses, 1996 December; triangles, 1997 June.

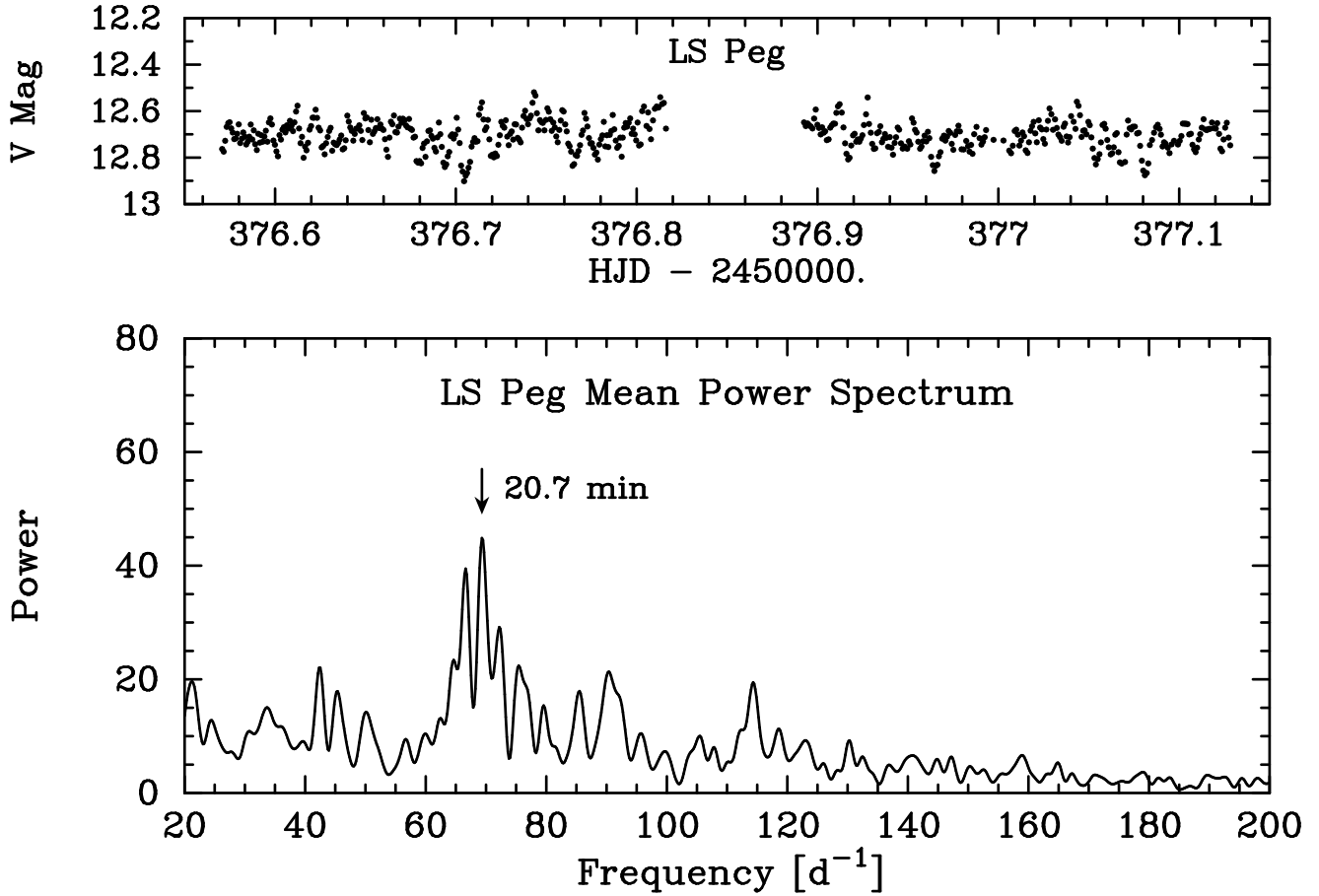


Fig. 3.— Upper frame: sample light curve of LS Peg. Lower frame: mean power spectrum of LS Peg from the 6 longest nights of photometry, with the main “QPO” signal marked with its period in minutes. The power in this signal corresponds to a full amplitude of 0.05 mag, but this must underestimate the actual amplitude, since the frequency rapidly wanders.

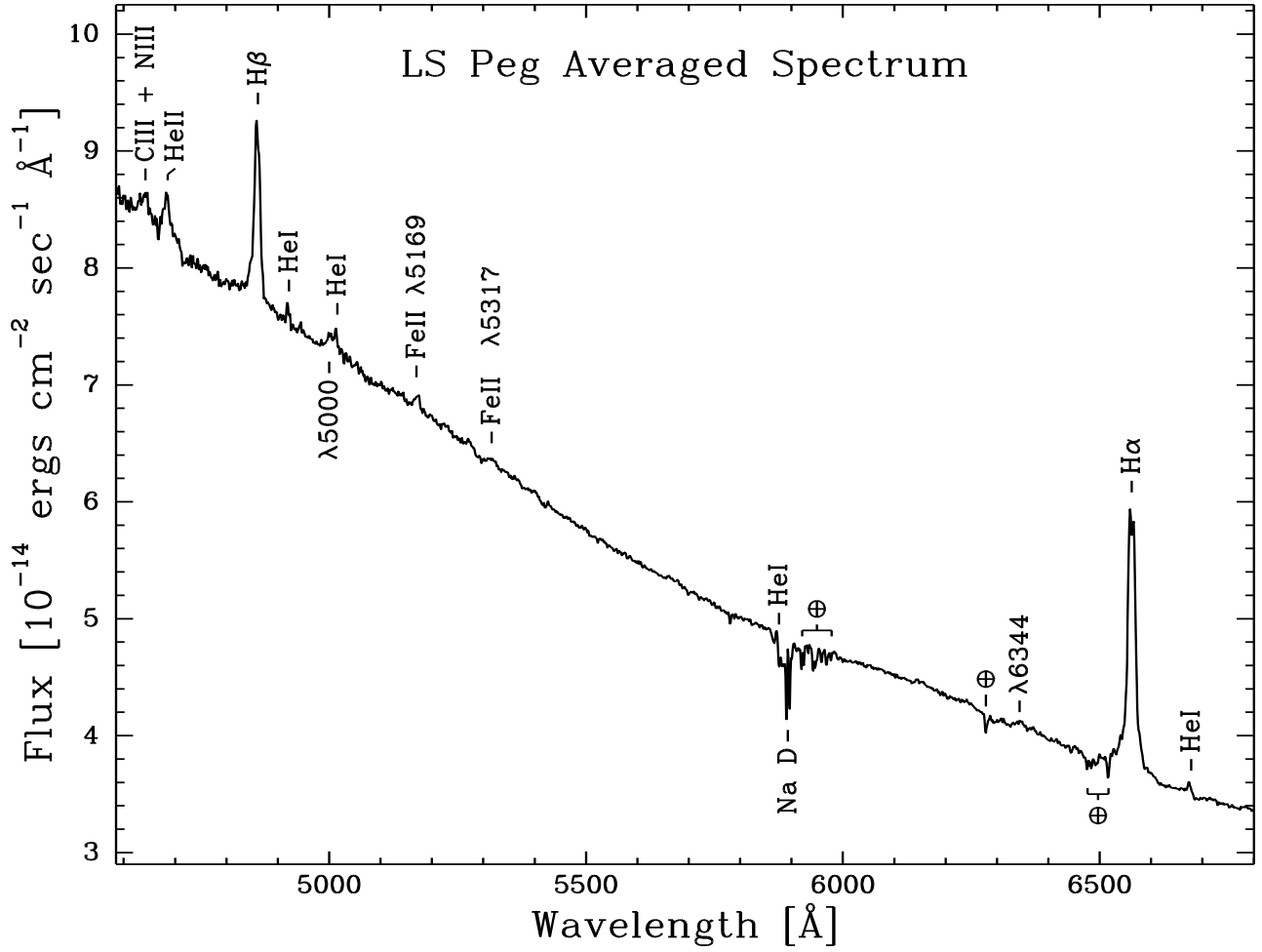


Fig. 4.— Averaged spectrum of LS Peg obtained in 1996 October. The telluric absorption lines have not been removed.

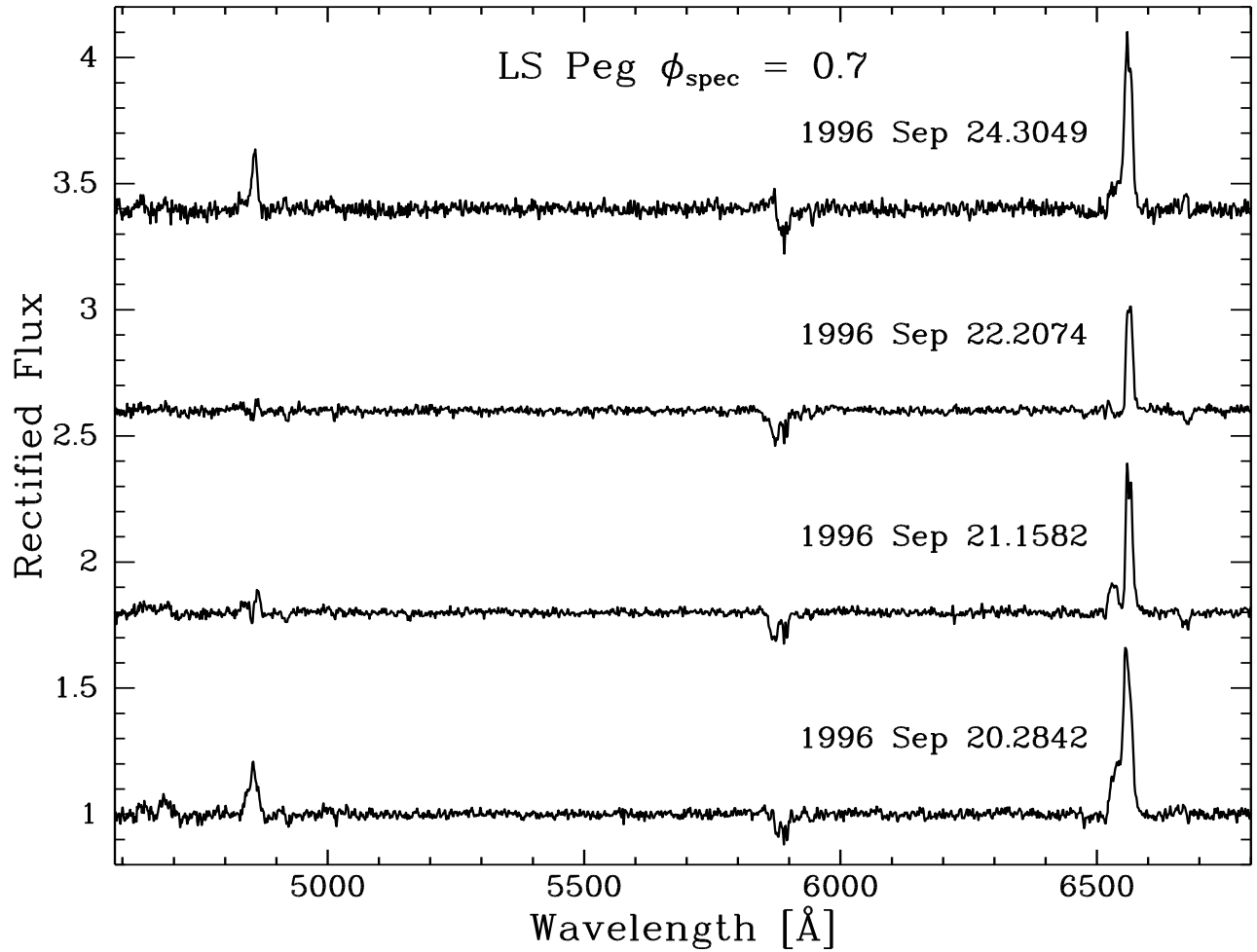


Fig. 5.— Rectified spectra of LS Peg from four different orbits at phase  $\phi = 0.7$ . Top three spectra are offset by a constant flux value. All four spectra were taken with the same telescope, detector, and chip combination.

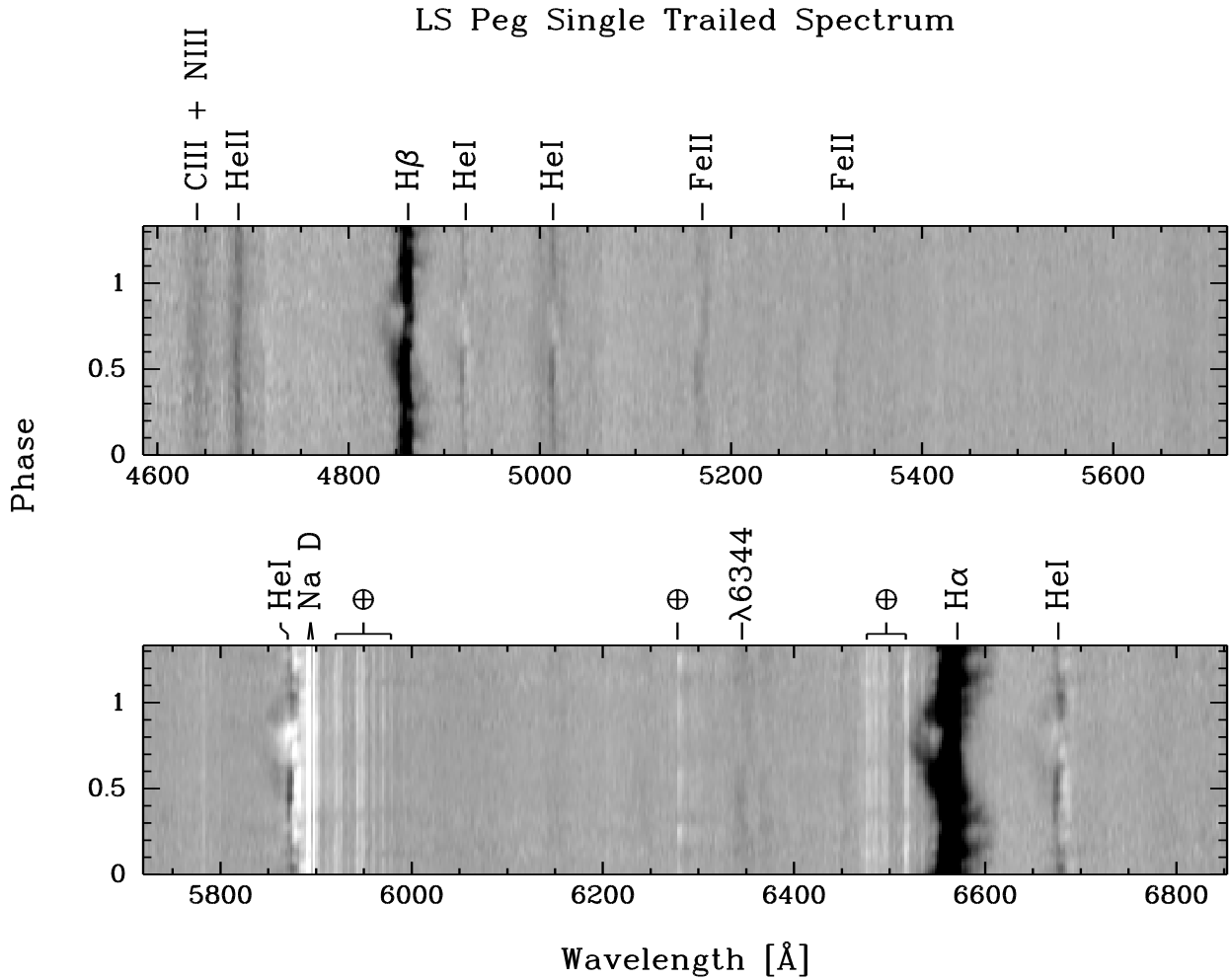


Fig. 6.— Single-trailed spectrum of LS Peg. One hundred fifty-five  $\sim 5$  min exposures from 1996 Sept. and Oct. are folded into 150 phase bins with a Gaussian phase smearing of  $\sigma = 0.02$  cycles. The first 50 bins are repeated for continuity. This is a negative image (black = emission). The telluric absorption lines have not been removed.

LS Peg HeI  $\lambda 5876$

Radial Velocity [ $\text{km s}^{-1}$ ]

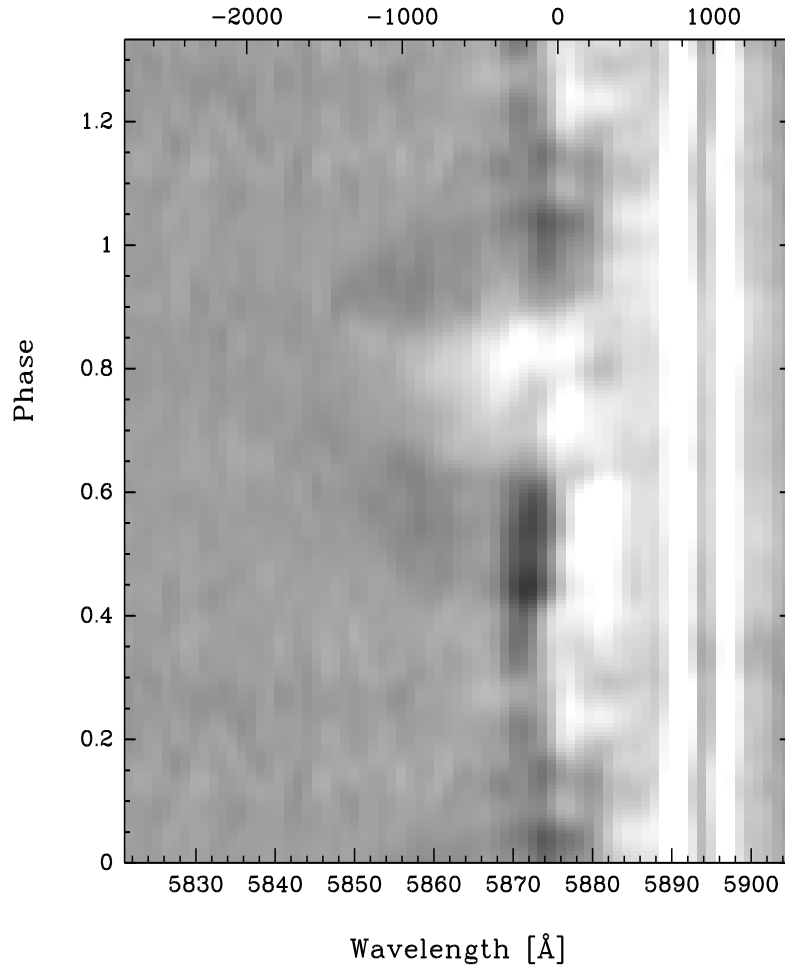


Fig. 7.— Detail of the He I  $\lambda 5876$  region of the single-trail spectrum. Bottom scale is wavelength in  $\text{\AA}$  and top scale is  $\lambda 5876$  radial velocity in  $\text{km s}^{-1}$ . The interstellar Na D lines are prominent. The broad, high-velocity, blueshifted emission occurs at the same phase as the blueshifted wings of the Balmer lines.

LS Peg H $\alpha$  & HeI

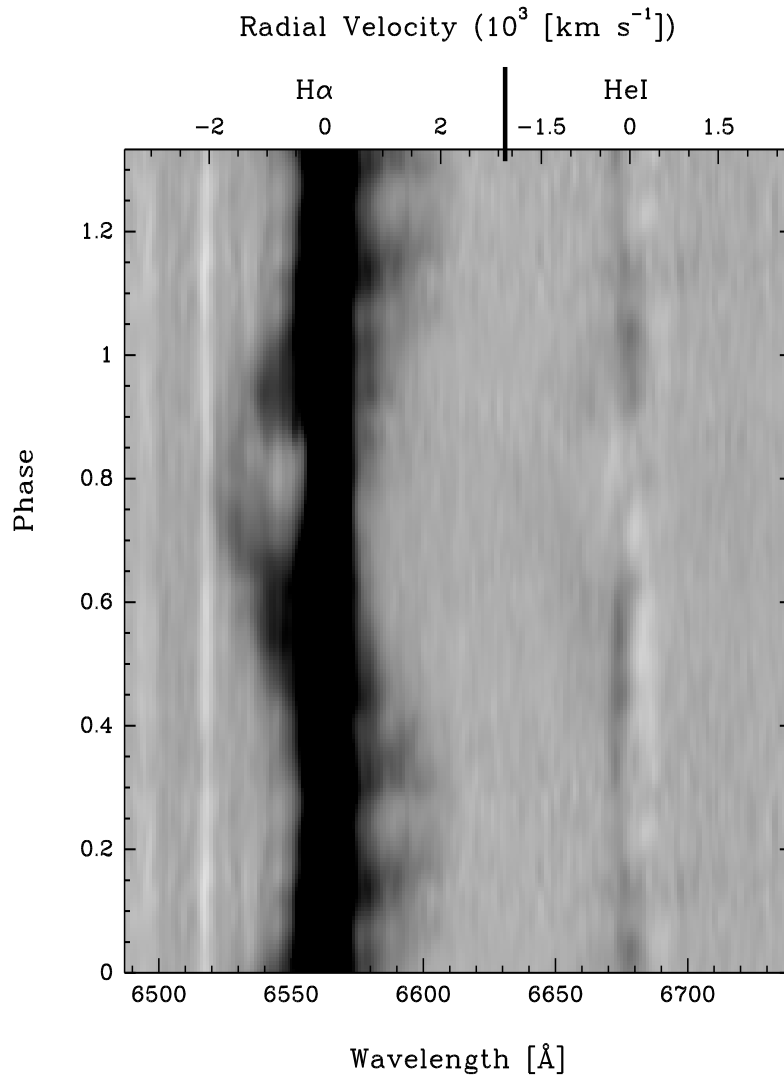


Fig. 8.— Detail of the H $\alpha$  and He I  $\lambda 6678$  region of the single-trail spectrum. Bottom scale is wavelength in  $\text{\AA}$  and top scale is radial velocity in  $10^3$  km s $^{-1}$ . The solid line separates the radial velocity scales for H $\alpha$  and He I. Note the terrestrial absorption line blueward of H $\alpha$ .



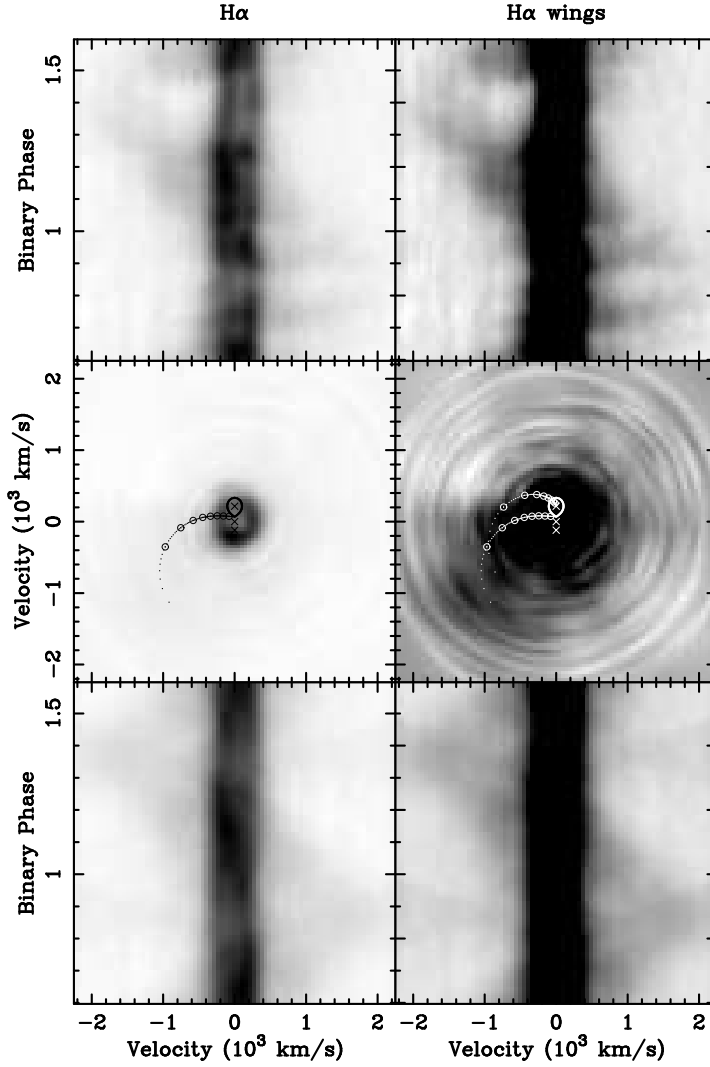


Fig. 9.—  $H\alpha$  single-trailed spectra (*top*), Doppler tomograms (*middle*), and predicted single-trailed spectra from the tomograms (*bottom*). The phasing of the spectra run from 0.6 to 1.6. The intensity in these negative images (black = emission) is adjusted in the left panels to emphasize the line core, while the right panels emphasize the line wings. Crosses mark the center of mass of the secondary (*top*), the system (*middle*), and the white dwarf (*bottom*). The secondary Roche lobe is outlined. On the left, the gas stream trajectory is plotted, while on the right, the upper trajectory is the Keplerian velocity of the disk along the gas stream and the lower trajectory is the gas stream.

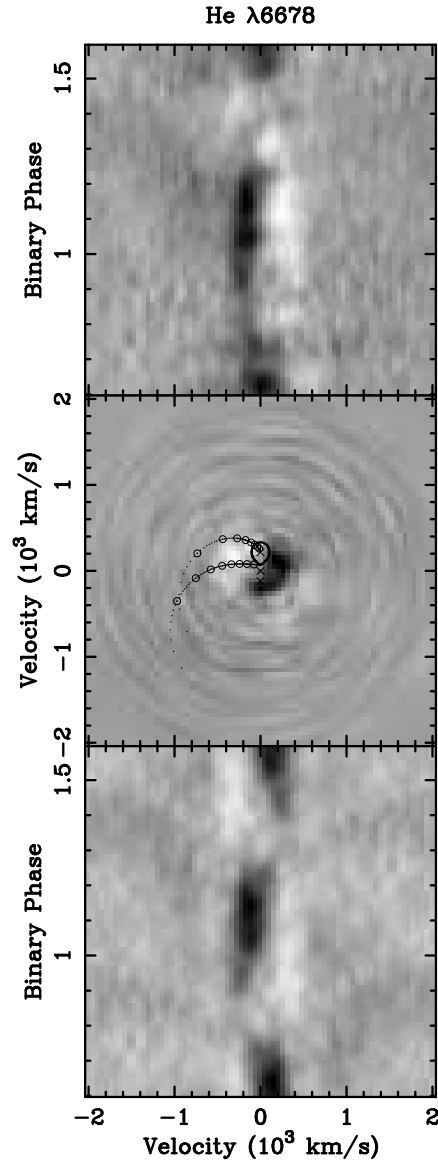


Fig. 10.— He I  $\lambda 6678$  single-trailed spectrum, Doppler tomogram, and predicted single-trailed spectrum with same conventions as Figure 9.

### LS Peg H $\alpha$ Data and Model

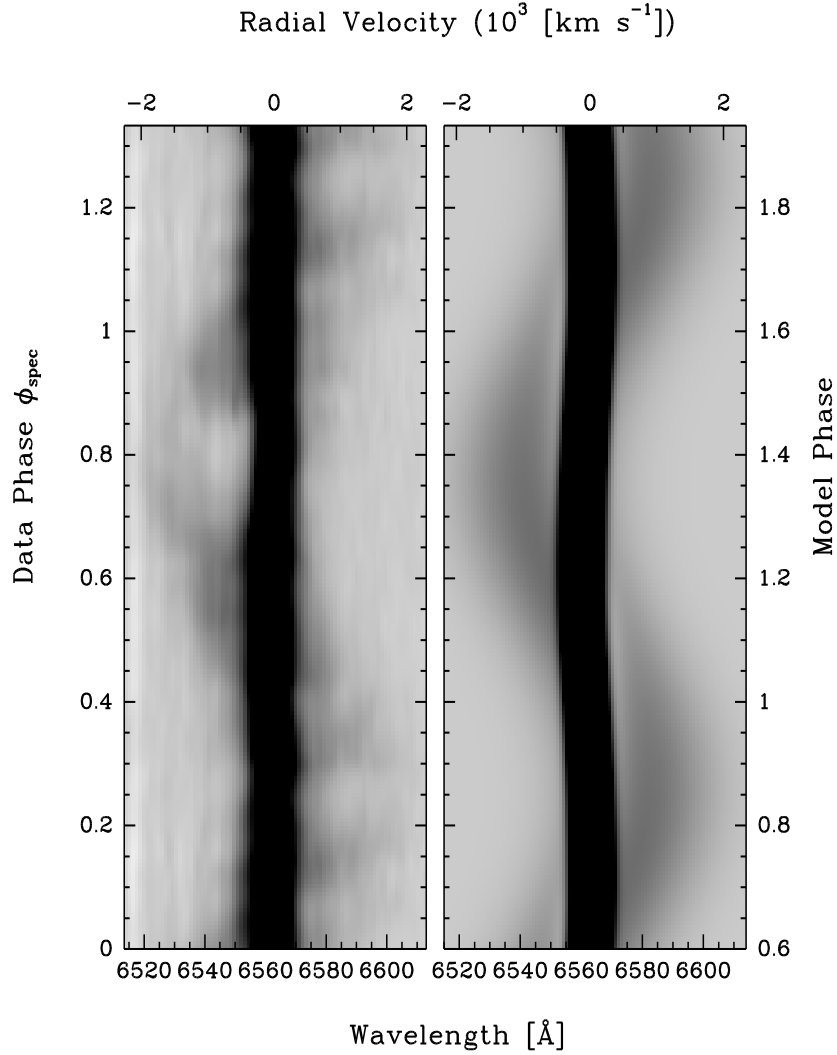


Fig. 11.— Comparison of the single-trailed H $\alpha$  spectrogram (*left*) with the disk-overflow model (*right*). The zero phase of the “data phase” is the blue-to-red crossing of the H $\alpha$  wings, while the zero phase of the model corresponds to the inferior conjunction of the secondary. Intensity is adjusted to emphasize the high-velocity wings.

### LS Peg H $\alpha$ Data and Model

Radial Velocity ( $10^3$  [km s $^{-1}$ ])

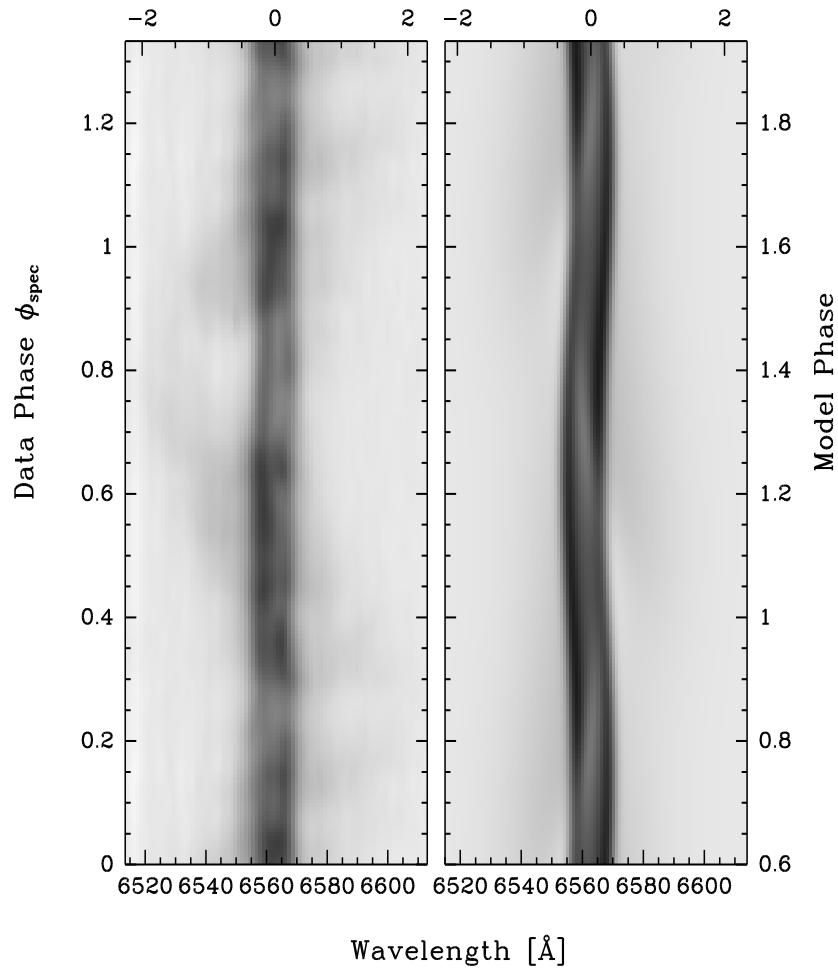


Fig. 12.— Same as Figure 11, but with the intensity adjusted to emphasize the line cores.

## LS Peg & PX And He I $\lambda 5015$

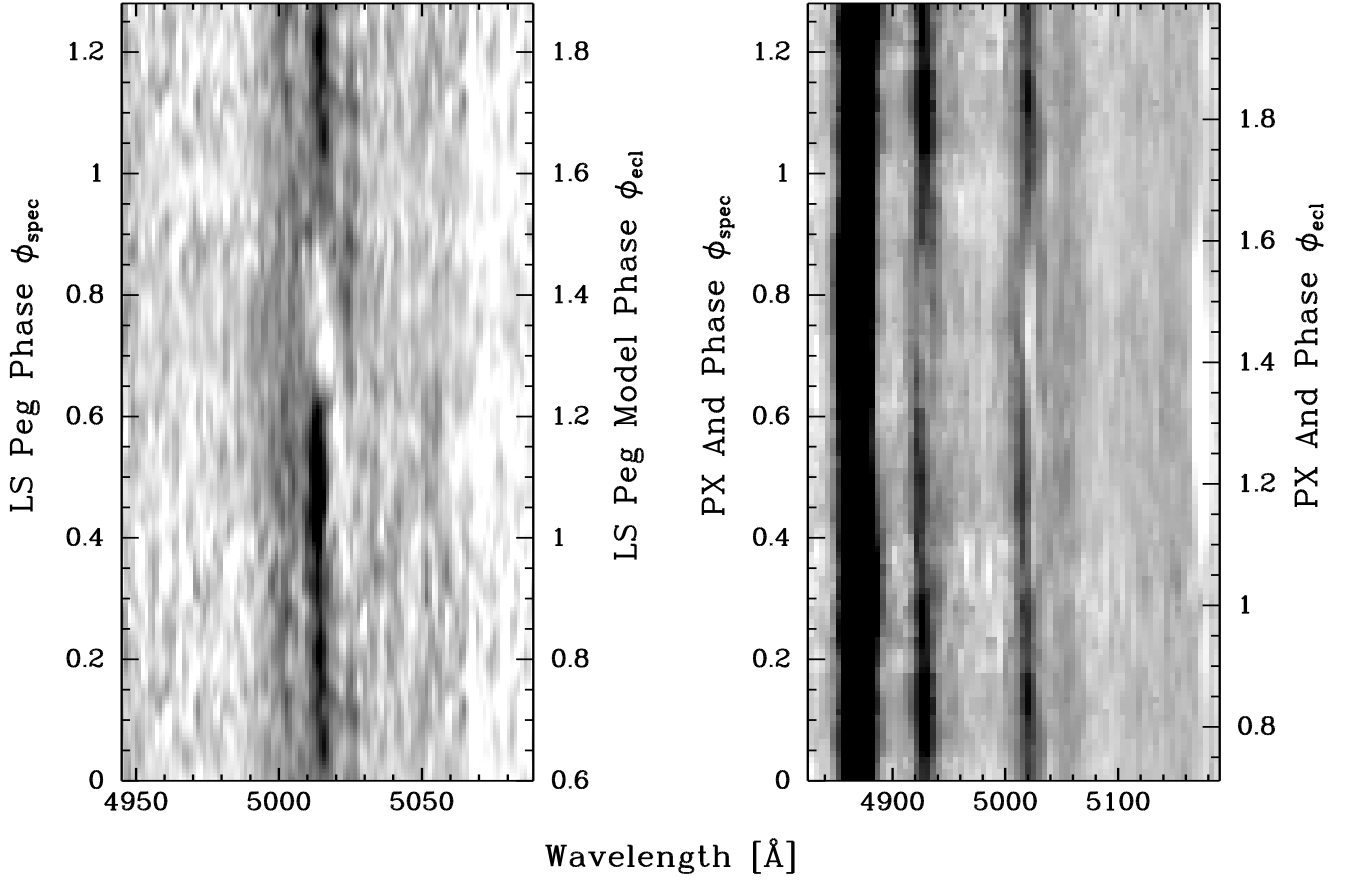


Fig. 13.— Comparison of LS Peg and PX And single-trailed spectra in the  $\lambda 5015$  region. Phase zero for  $\phi_{\text{spec}}$  corresponds to the blue-to-red crossing of  $\text{H}\alpha$  and phase zero for  $\phi_{\text{ecl}}$  corresponds to the eclipse. The PX And data were previously published by Thorstensen et al. (1991) and are folded into 100 phase bins with a Gaussian phase smearing of  $\sigma = 0.02$  cycles.